https://doi.org/10.5194/egusphere-2025-1515
Preprint. Discussion started: 24 April 2025

Gross primary productivity responses to meteorological drivers: insights from observations and multi-model ensembles

Yuxin Zheng [1], Xu Yue [1*], Xiaofei Lu [1], Jun Zhu [1]

[1] Jiangsu Key Laboratory of Atmospheric Environment Monitoring and Pollution Control, Collaborative Innovation Center of Atmospheric Environment and Equipment Technology, School of Environmental Science and Engineering, Nanjing University of Information Science & Technology (NUIST), Nanjing, 210044, China

[*] Corresponding authors: Xu Yue (yuexu@nuist.edu.cn)

Abstract

Climate change has a substantial impact on ecosystem gross primary productivity (GPP), but the specific roles of different meteorological factors across various vegetation types remain unclear. This study investigates GPP responses to variations in temperature, precipitation, and drought, using data from three observational products and 17 dynamic vegetation models. Observed GPP showed a positive response to temperature in boreal regions, with sensitivities ranging from 0.01 to 0.05 g C m^2 day^{-1} K^{-1}. In contrast, GPP responded negatively to temperature in the tropics, with sensitivities of -0.07±0.15 g C m^2 day^{-1} K^{-1} for evergreen broadleaf forests and -0.25 ± 0.11 g C m^2 day^{-1} K^{-1} for C_4 grasslands. Precipitation had a relatively low impact on GPP in deciduous and evergreen forests, while non-tree species, such as grasslands and croplands, showed a positive response. GPP sensitivity to drought index (scPDSI) was similar to that of precipitation, except that observed GPP in evergreen forests negatively responded to scPDSI. The models generally reproduced these observed patterns but tended to overestimate the effect of precipitation on GPP. As a result, they predicted higher sensitivity in tropical grasslands to drought stress but lower resilience in trees. Both observations and simulations exhibited negative GPP responses to extreme warming and drought on a global scale, though models tended to overestimate the magnitude of these negative effects. This study distinguished GPP responses to key meteorological factors across vegetation types and numerical models, providing critical insights for improving the prediction of terrestrial carbon sinks and promoting the climatic resilience of ecosystems.

Keywords: Gross primary productivity; multi-model ensemble; sensitivity; meteorology; drought

https://doi.org/10.5194/egusphere-2025-1515
Preprint. Discussion started: 24 April 2025

1 Introduction

Gross primary productivity (GPP) is a critical metric of ecosystem's ability to capture and convert atmospheric carbon dioxide into biomass through photosynthesis, providing the primary carbon input for ecosystems (Fernandez-Martinez et al., 2017; Pinker et al., 2010; Xiao et al., 2019). Therefore, GPP drives key ecosystem processes such as respiration and vegetation growth, which are the foundation of the global carbon cycle (Beer et al., 2010). A variety of environmental and climatic stressors, such as warming and drought, exert a substantial influence on GPP (Tian et al., 2021; Zhang et al., 2022; Liu et al., 2014). Understanding these interactions is vital for predicting ecosystem responses to ongoing and future climate changes, as well as for managing carbon sequestration efforts across diverse biomes.

Climatic factors substantially influence GPP, especially for temperature and precipitation. Temperature affects plant enzymatic activity, generally increasing photosynthetic rates with rising temperatures (Tang et al., 2022). However, this relationship is not linear and can vary across regions. For instance, multi-model simulations show a negative sensitivity of GPP to temperature in tropical regions, with an average sensitivity of -2.2±1.2 Pg C yr^{-1} K^{-1} (Piao et al., 2013). Precipitation is also a major determinant, affecting water availability and stomatal behavior in plants. Insufficient precipitation may enhance water stress, leading to stomatal closure and reduced photosynthetic rates, thereby decreasing GPP (Liang et al., 2024a). The GPP responses to these climatic factors also vary by plant species. For instance, coniferous forests are more sensitive to temperature and soil moisture, whereas broad-leaved forests are more affected by light and soil nitrogen content (Feng et al., 2007).

As a compound weather extreme, drought typically has negative impacts on GPP by imposing water stress. During drought, plants often close their stomata to conserve water, which reduces CO_2 uptake and slows photosynthesis (Granier et al., 2007). While this response is protective in the short term, it ultimately leads to a decline in GPP. Furthermore, reduced soil moisture under drought conditions limits water availability for plant roots, exacerbating water stress and further impairing photosynthesis (Chen and Dominguez, 2024; Brunner and Chartier‐Rescan, 2024). Over the past three decades, there has been a notable increase in the sensitivity of global vegetation productivity to drought conditions. For example, Wei et al. (2023) found that the sensitivity of GPP to drought rose by 13.76% in 2006-2018 compared to 1993-2005. This growing sensitivity indicates that, as droughts become more frequent and severe with climate change (Zscheischler et al., 2014), their impacts on GPP could significantly alter the global carbon cycle, potentially reducing the ability of ecosystems to function as carbon sinks.

Vegetation models are essential for estimating GPP and predicting its future trends under different climate scenarios. These models simulate key processes like vegetation growth, photosynthesis, and carbon cycling, providing valuable insights into how GPP may respond to environmental changes (Piao et al., 2013; Yue et al., 2024). However, large uncertainties arise due to differences in model structures, algorithms, and parameter settings (Poulter et al., 2014; Zhang et al., 2018). To address these, the multi-model ensemble approach has emerged as a promising strategy. For example, the Global Carbon Project (GCP) utilized the ensemble mean of 16 models to estimate land carbon sinks over the past century (Friedlingstein et al., 2022). By integrating models with different structures and parameterizations, this approach reduces model-specific biases and enhances the accuracy of ecosystem simulations. Nevertheless, it can also amplify common biases across models. For instance, Piao et al. (2013) found that process-based models

https://doi.org/10.5194/egusphere-2025-1515
Preprint. Discussion started: 24 April 2025

tend to overestimate the effect of precipitation on GPP while underestimate the response of net primary productivity (NPP) to temperature changes. This underscores the need of careful calibration and validation using observed data to improve model reliability.

In this study, we aim to address these challenges by evaluating GPP responses to key climatic factors using a multi-model ensemble approach. We analyze outputs from 17 vegetation models participating in the TRENDY project (Sitch et al., 2024) in support of the GCP. We focus on how well these models reproduce observed relationships between GPP and climatic variables such as temperature, precipitation, and drought. In addition, we compare the simulated GPP sensitivities across models and plant functional types (PFTs). We seek to enhance our understanding of the complex interactions between climatic factors and GPP, ultimately providing more reliable projections of ecosystem responses to future climate change.

2 Methods and data

2.1 Observations of GPP

This study validates models using three GPP observational datasets. The Global Land Surface Satellite (GLASS) dataset provides a global GPP product from 1981 to 2017 at a spatial resolution of 0.05º (Liang et al., 2013). It integrates data from the Moderate Resolution Imaging Spectroradiometer (MODIS) and Advanced Very High Resolution Radiometer (AVHRR), using optimized light-use efficiency models to estimate GPP by combining absorbed PAR with environmental factors such as leaf area index and shortwave radiation (Liang et al., 2024b). The GLASS dataset has been validated against ground measurements and aligns well with observed GPP, capturing seasonal and interannual variability across ecosystems (Ma and Liang, 2022).

The Global Ozone Monitoring Experiment Solar-Induced Fluorescence (GOSIF) dataset provides global GPP derived from solar-induced chlorophyll fluorescence (SIF), a proxy for photosynthetic activity. This dataset is produced using machine learning approach that integrates discrete SIF measurements from the Orbiting Carbon Observatory-2 (OCO-2) with continuous spatial and temporal data from the Enhanced Vegetation Index (EVI) obtained from MODIS, and meteorological reanalysis data from Modern-Era Retrospective analysis for Research and Applications, Version 2 (MERRA-2) (Li and Xiao, 2019). GOSIF provides GPP data at 0.05º spatial resolution and 8-day intervals from 2001 to 2018.

The third dataset, short as JUNG, is a benchmark global product that estimates GPP using the Model Tree Ensemble algorithm (Jung et al., 2011). This dataset integrates satellite vegetation indices and flux measurements from the FLUXNET network, providing global coverage at 0.5º spatial resolution and spanning from 1982 to 2011. The JUNG GPP product has been extensively validated against flux tower measurements, ensuring accurate spatiotemporal GPP estimates (Jung et al., 2009). It has been widely used in climate and carbon cycle modeling, offering valuable insights into the impacts of climate change on global vegetation productivity (Wu et al., 2021; Harper et al., 2018; Leng et al., 2024).

2.2 Model data from the TRENDY project

TRENDY, which stands for “Trends and drivers of the regional scale terrestrial sources and sinks of carbon dioxide”, investigates changes in land carbon fluxes using a multi-model ensemble approach (Le Quéré et al., 2018; Zeng et al., 2022). For 2022, the project (TRENDY v-11)

https://doi.org/10.5194/egusphere-2025-1515
Preprint. Discussion started: 24 April 2025

involves a total of 17 Dynamic Global Vegetation Models (DGVMs, Table 1), all driven by the same forcing data including CO_2 concentrations, meteorological reanalyses, and land use change (LUC). TRENDY examines various aspects such as model structures, parameter settings, input data quality, and the consistency of simulation results. The models follow standardized experimental protocols to isolate the effects of CO_2 fertilization, climate change, and LUC on global carbon cycle variations (Sitch et al., 2024). Four sets of simulations were performed for each model with different combinations of time-varying forcings. The S0 run serves as a control simulation with all forcings fixed to pre-industrial period. The S1 run is similar to S0 but applies observed CO_2 concentrations. The S2 run builds on S1 by incorporating year-to-year variations in meteorological forcing. The S3 run allows all forcings (CO_2, climate, and land use) to evolve over time, reflecting the real-world environmental changes. For this study, we analyzed simulated GPP data from the 17 DGVMs for the S2 and S3 experiments, focusing on GPP responses to changes in major meteorological variables.

2.3 Drought index and meteorological data

The self-calibrating Palmer Drought Severity Index (scPDSI) is an improved version of the original PDSI and is widely recognized for its application in drought monitoring and assessment (Wells et al., 2004). The scPDSI enhances the traditional PDSI by incorporating a self-calibration mechanism that evaluates and adjusts based on past drought events, improving both the accuracy and stability of the index. Like the original PDSI, the scPDSI relies on time series of precipitation and temperature, along with location-specific parameters related to soil and surface properties. However, it introduces updated calculation methods and utilizes more extensive historical meteorological data to establish baseline moisture conditions for each period (Van Der Schrier et al., 2013). This self-calibration enables the scPDSI to more accurately reflect drought trends and intensities across regions, removing dependency on fixed parameters and baseline periods that limit the traditional PDSI. In this study, scPDSI data are sourced from the Climatic Research Unit (CRU), derived from monthly precipitation and temperature fields in the CRU TS 2.1 high-resolution surface climate dataset, covering the period from 1901 to 2022 with a spatial resolution of 0.5°×0.5°. The scPDSI values typically range from -4 to 4, with more positive (negative) values representing wetter (drier) conditions.

In addition to the drought index, we used meteorological reanalyses of ERA-5 developed by the European Centre for Medium-Range Weather Forecasts (ECMWF). ERA-5 represents a major advance in modeling and data assimilation techniques, combining global observational data with state-of-the-art model outputs to produce a comprehensive and consistent global dataset (Sun et al., 2020). This dataset offers hourly estimates at a horizontal resolution of 30-km, with 137 vertical levels extending from the surface to 80 km in the atmosphere. ERA-5 serves as a crucial resource for applications in climate research, weather forecasting, environmental monitoring, and policy-making (Wang et al., 2024; Muñoz-Sabater et al., 2021; Jiao et al., 2021). For this study, we used ERA-5 surface meteorological variables, including 2-meter air temperature (T2M) and total precipitation (PRE).

Table 1 Summary of models participating in the TRENDY project.

MODEL	CABLE-POP	CLASSIC	CLM5.0	DLEM	IBIS	JSBACH	ISAM	JULES	
Country	Australia	Canada	USA	USA	China	Germany	USA	UK	
Resolution	1°×1°	1°×1°	1.25°×1°	0.5°×0.5°	1°×1°	1.875°×1.875°	0.5°×0.5°	1.875°×1.25°	
Carbon–nitrogen interactions	YES	NO	YES	YES	NO	YES	YES	YES	
Separation of direct and diffuse radiation	YES	NO	YES	NO	NO	NO	NO	YES	
Reference	(Haverd et al., 2013)	(Melton et al., 2020)	(Lawrence et al., 2019)	(Tian et al., 2015)	(Kucharik et al., 2000)	(Reick et al., 2021)	(Jain and Yang, 2005)	(Clark et al., 2011)	
MODEL	LPJ	LPJ-GUESS	LPX-Bern	OCN	ORCHIDEE	SDGVM	VISIT	VISIT-NIES	YIBs
Country	USA	Germany	Switzerland	Germany	France	USA	Japan	Japan	China
Resolution	0.5°×0.5°	0.5°×0.5°	0.5°×0.5°	1°×1°	0.5°×0.5°	1°×1°	0.5°×0.5°	0.5°×0.5°	1°×1°
Carbon–nitrogen interactions	NO	YES	YES	YES	YES	YES	NO	NO	NO
Separation of direct and diffuse radiation	NO	NO	NO	NO	NO	NO	NO	NO	YES
Reference	(Sitch et al., 2003)	(Smith et al., 2001)	(Spahni et al., 2013)	(Zaehle and Friend, 2010)	(Krinner et al., 2005)	(Walker et al., 2017)	(Kato et al., 2013)	(Ito, 2010)	(Yue and Unger, 2015)

https://doi.org/10.5194/egusphere-2025-1515
Preprint. Discussion started: 24 April 2025

https://doi.org/10.5194/egusphere-2025-1515
Preprint. Discussion started: 24 April 2025

2.4 Land cover data

The MODIS vegetation cover dataset was used to determine the dominant land cover types for individual grid cells. This dataset analyzes vegetation reflectance in the visible and near-infrared wavelengths to produce essential vegetation indices, such as the Normalized Difference Vegetation Index (NDVI) and EVI (Friedl et al., 2010), offering comprehensive global coverage with a fine spatial resolution up to 250m and an 8-day temporal interval (Huete et al., 2002). The MODIS vegetation cover dataset has been widely used in research areas including ecological monitoring, agricultural and forestry management, climate change studies, and disaster assessment (Shim et al., 2014; Wu et al., 2019; Wang et al., 2022). For this study, we used MODIS land cover data version 051, averaged for 2001-2012, to classify dominant vegetation types across seven categories: C_3 grassland (C3G), shrubland (Shr), deciduous broadleaf forest (DBF), evergreen broadleaf forest (EBF), evergreen needleleaf forest (ENF), cropland (Crop), and C_4 grassland (C4G).

2.5 Statistical methods

To explore the relationships between variables, we applied three statistical techniques: Pearson correlation, partial correlation, and linear regression. The Pearson correlation coefficient γ was calculated to assess the linear relationship between two variables and is defined as follows:

$$\gamma = \frac{\sum (X_i - \overline{X})(Y_i - \overline{Y})}{\sqrt{\sum (X_i - \overline{X})^2 \sum (Y_i - \overline{Y})^2}}$$

where X_i is GPP and Y_i is one of meteorological variables. $\overline{X}$ and $\overline{Y}$ are their mean values.

We conducted a multivariate partial correlation analysis to exclude the potential confounding effects of other meteorological factors (Zhou et al., 2016; Zhang et al., 2023). For example, the correlation of γ_{12} between GPP and PRE is not only affected by the relationships between GPP and other meteorological variables, such as T2M (γ_{13}), but also the relationships between PRE and T2M (γ_{23}). As a result, the partial correlation coefficient $\gamma_{12\cdot3}$ is calculated as follows:

$$\gamma_{12\cdot3} = \frac{\gamma_{12} - \gamma_{13}\gamma_{23}}{\sqrt{(1-\gamma_{13}^2)(1-\gamma_{23}^2)}}$$

This method ensures that the relationship between GPP and PRE is independent of the effects of T2M, providing a better quantification of their direct associations.

To assess the dependency of GPP on multiple meteorological variables, we applied a multiple linear regression method. This approach allows us to estimate the individual contributions of each predictor to GPP while controlling the influence of other factors. The multiple linear regression model is formulated as:

$$Y = \beta_0 + \beta_1 X_1 + \beta_2 X_2 + \epsilon$$

where Y represents GPP, X_1 and X_2 denote PRE and T2M respectively. Here, β_0 is the intercept, and β_1, β_2 are the regression coefficients associated with each predictor. These coefficients represent the partial effect of each variable on GPP while holding other variables constant. The term ϵ accounts for the variability in GPP not explained by the predictors. We assessed the significance of each coefficient to determine the strength and direction of the relationships between GPP and individual predictors (PRE or T2M). We also quantify changes in GPP during years of extreme warming or drought, relative to the mean state. Extreme warming episodes are

https://doi.org/10.5194/egusphere-2025-1515
Preprint. Discussion started: 24 April 2025

identified as years when grid-specific temperatures exceed the 90th percentile, while drought extremes are defined as years when the scPDSI falls below the 10th percentile. To facilitate the analyses, we interpolated all datasets, including GPP observations, TRENDY simulations, ERA-5 meteorology, scPDSI, and MODIS land cover, into the same resolution of $1^{o} \times 1^{o}$.

3 Results

3.1 Spatiotemporal variations of GPP

We first compared the temporal variations of GPP between observations and simulations (Fig. 1a). Observed GPP from GLASS showed a global mean of 123.73 Pg yr^{-1} and a positive trend of 0.18 Pg yr^{-2} during 1982-2017. Simulated GPP from the S3 run of the TRENDY project exhibited large inter-model variability, ranging from 95.44 Pg yr^{-1} in CABLE-POP to a maximum of 151.65 Pg yr^{-1} in JULES. Most models predicted positive trends between 0.17 and 0.53 Pg yr^{-2}. The multi-model ensemble (MME) produced an average GPP of 120.06 Pg yr^{-1}, closely matching the GLASS observations. However, the ensemble simulations yielded a positive trend of 0.37 Pg yr^{-2}, almost doubling the estimate with GLASS. In addition to the overall trend, observations showed substantial year-to-year variations with a standard deviation of 3.16 Pg yr^{-1}, while models in general underestimated this interannual variations, ranging from 1.84 to 5.75 Pg yr^{-1}.

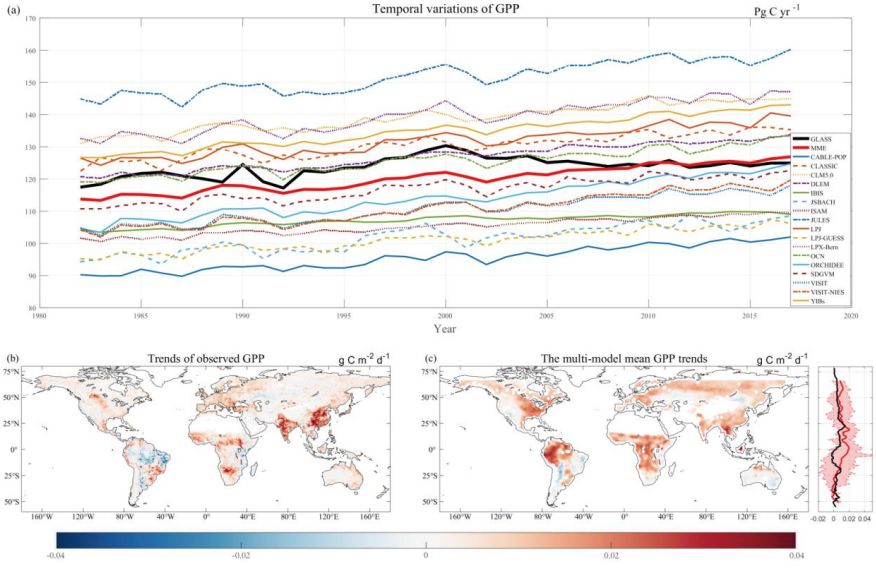

Fig. 1. Comparison of spatiotemporal variations in Gross Primary Productivity (GPP) between observations and model simulations. The (a) temporal variations in simulated GPP from individual models and the multi-model ensemble (MME) mean (thick red line) are shown alongside observational data from GLASS (thick black line). Spatial patterns of GPP trends from (b) observations, represented as the mean of three products (GLASS, GOSIF, JUNG), are compared with (c) the MME of the simulations. Latitudinal variations in GPP trends are also shown, with observational data represented in black and model simulations in red; shading indicates one standard deviation.

https://doi.org/10.5194/egusphere-2025-1515
Preprint. Discussion started: 24 April 2025

The ensemble of three observational datasets revealed large spatial heterogeneity in GPP trends (Fig. 1b). The greatest GPP enhancement occurred around 25° N, largely driven by hotspots in eastern China and India. Positive trends were also observed in the Sahel, southern Africa, Eurasia, and North America. In contrast, GPP in South America, particularly within the Amazon rainforest, showed a decreasing trend. Similarly, the MME predicted positive GPP trends across much of the Northern Hemisphere (NH, Fig. 1c), though model simulations underestimated the GPP increases observed in China and India. Nevertheless, model predictions yielded a notable positive trend in South America, where observations suggested a decline. Overall, the MME captured the latitudinal variations in GPP trends but tended to overestimate positive trends in tropical regions.

3.2 Relationships between GPP and meteorological factors

We analyzed the relationships between GPP and meteorological variables, including temperature, precipitation, and drought indices (Fig. 2). Observed GPP showed positive responses to temperature at high latitudes of NH but negative responses at lower latitudes, particularly in the Southern Hemisphere (SH). Warming promotes GPP at high latitudes by moving temperature closer to the optimal range for photosynthesis, while inhibiting GPP at lower latitudes where temperatures often exceed this threshold (Piao et al., 2013). The MME well reproduced this spatial pattern, reflecting positive correlations in the boreal regions and negative correlations in the tropics (Fig. 2a). Precipitation was positively correlated with GPP across most tropical and subtropical areas, especially in arid and semi-arid regions dominated by shallow-rooted vegetation. In contrast, negative correlations between GPP and precipitation were observed at high latitudes in the NH (>50° N), where GPP variations depend strongly on solar radiation. Increased rainfall reduces sunlight availability, inhibiting photosynthesis and resulting in negative correlations between GPP and precipitation. While the MME generally captured the observed positive correlations between GPP and precipitation (Fig. 2b), it did not predict the negative correlations north of 50° N, likely due to an inadequate representation of light dependency in those regions. GPP was positively correlated with scPDSI in low to middle latitudes but negatively correlated in boreal regions, mirroring precipitation trends and highlighting precipitation's role in GPP responses to drought. The MME reproduced these patterns but tended to overestimate positive correlations, especially in EBF (Fig. 2c).

We then distinguished the relationships between GPP and meteorological factors across various products/models and vegetation types (Figs. 3 and S1-S3). Observed GPP correlations with temperature were insignificant for most vegetation types, with the exception of positive correlations for ENF and negative correlations for C4G (Fig. 3a). The TRENDY models largely captured these relationships, with 12 out of 17 models yielding positive correlations for ENF and 14 out of 17 showing negative correlations for C4G. Observed correlations with precipitation were generally positive, especially for C3G and C4G (Fig. 3b). Among the 17 models, 9 predict significantly positive correlations for both C3G and C4G, suggesting a consistent parameterization of water stress for these grass species. Positive correlations were more common with drought indices, particularly for C3G, C4G, Shr, and Crop (Fig. 3c). These patterns were well captured by the TRENDY models, though they tended to predict positive and mostly significant responses for EBF, where observed GPP had very low correlations with scPDSI.

https://doi.org/10.5194/egusphere-2025-1515
Preprint. Discussion started: 24 April 2025

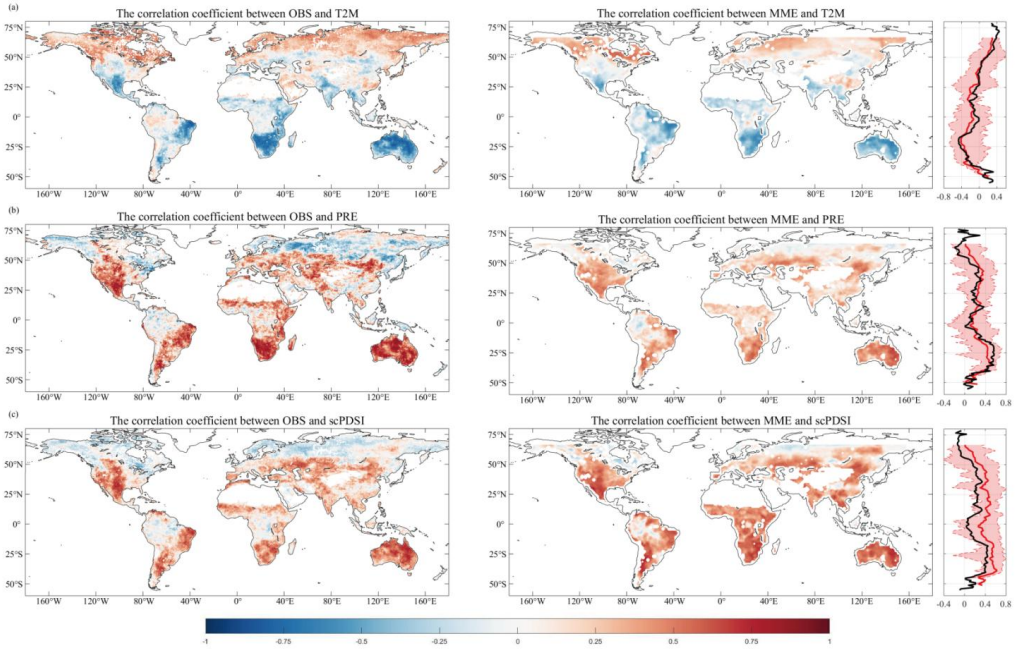

Fig. 2. Mean spatial correlation coefficients between GPP and meteorological variables. The correlation between annual GPP and (a) temperature (T2M), (b) precipitation (PRE), and (c) self-calibrated Palmer Drought Severity Index (scPDSI) is averaged for observational datasets (GLASS, GOSIF, JUNG) and multiple model ensemble simulations. For observed GPP, correlation coefficients were calculated at each grid cell over the period 1982-2017 for GLASS, 2001-2018 for GOSIF, and 1982-2011 for JUNG. For simulated GPP, correlation coefficients were calculated at each grid cell over the period 1982-2017 for individual models. Latitudinal variations in correlation coefficients are also shown, with observational data represented in black and model simulations in red; shading indicates one standard deviation.

https://doi.org/10.5194/egusphere-2025-1515
Preprint. Discussion started: 24 April 2025

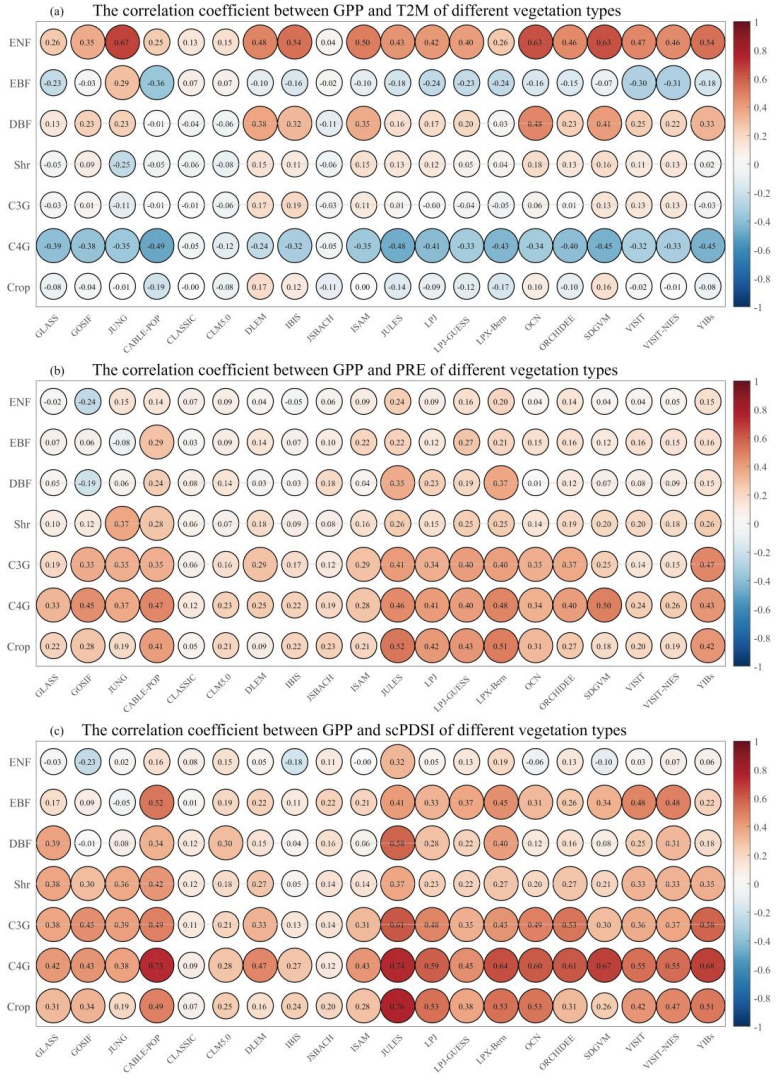

Fig. 3. Heatmaps of Pearson correlation coefficients between GPP and meteorological variables across vegetation types. Panels show correlations between GPP and (a) T2M, (b) PRE, and (c) scPDSI for three observational data products (GLASS, GOSIF, and JUNG) and 17 vegetation models. Vegetation types include evergreen needleleaf forest (ENF), deciduous broadleaf forest (DBF), evergreen broadleaf forest (EBF), shrubland (Shr), C_3 grassland (C3G), C_4 grassland (C4G), and cropland (Crop). Correlation coefficients are represented by circles, with larger circles indicating significant correlations (P<0.05) and smaller circles indicating non-significant correlations (P>0.05).

https://doi.org/10.5194/egusphere-2025-1515
Preprint. Discussion started: 24 April 2025

We further conducted partial correlation analysis to isolate the independent effects of individual meteorological variables. For temperature, observed and simulated GPP showed consistently positive correlations for ENF and DBF, but negative correlations for C4G (Fig. S4a). For other vegetation types, observed GPP displayed slightly positive but statistically insignificant correlations, while model simulations generally showed stronger correlations except for EBF, where negative correlations were achieved. Precipitation exhibited positive correlations with GPP for C3G, C4G, Shr, and Crop, with stronger correlations in the model simulations compared to observations (Fig. S4b). For tree species, observations suggested weak correlations between precipitation and GPP, whereas the models predicted positive correlations. Consequently, the models showed strong positive GPP responses to scPDSI (Fig. S4c), likely due to the enhanced amelioration in GPP by precipitation (Fig. S4b). On average, the partial correlation coefficients between GPP and meteorological variables were 52.02% lower than the direct correlations, indicating the non-negligible influences of interactions among meteorological factors.

We quantified the sensitivities of GPP to meteorological factors for both observations and models (Fig. 4). Results showed that one-degree increase in temperature generally led to an increase of 0.013-0.1g C m^2 day^{-1} in GPP across most vegetation types. However, GPP for EBF and C_4 grasslands decreased in response to rising temperatures. Notably, in C_4 grasslands, observed and simulated GPP showed negative responses to temperature, with sensitivities of -0.25 and -0.35 g C m^2 day^{-1} K^{-1}, respectively (Fig. 4a). Observed GPP showed low sensitivity to precipitation changes for trees (e.g., DBF, ENF, and EBF), but notably positive responses for non-tree (e.g., C3G, C4G, shrub, and crop) species (Fig. 4b). Models reproduced the larger responses of non-tree species compared to trees, though they tended to overestimate the impact of precipitation on GPP. The sensitivity of GPP to the drought index resembled that to precipitation, except that observed GPP negatively responded to scPDSI for ENF (Fig. 4c). Simulated GPP showed positive responses to drought index across all vegetation types, with the strongest sensitivity for C4G. In summary, the models effectively captured the high sensitivity of tropical grasslands to drought stress but underestimated the resilience of trees.

https://doi.org/10.5194/egusphere-2025-1515
Preprint. Discussion started: 24 April 2025

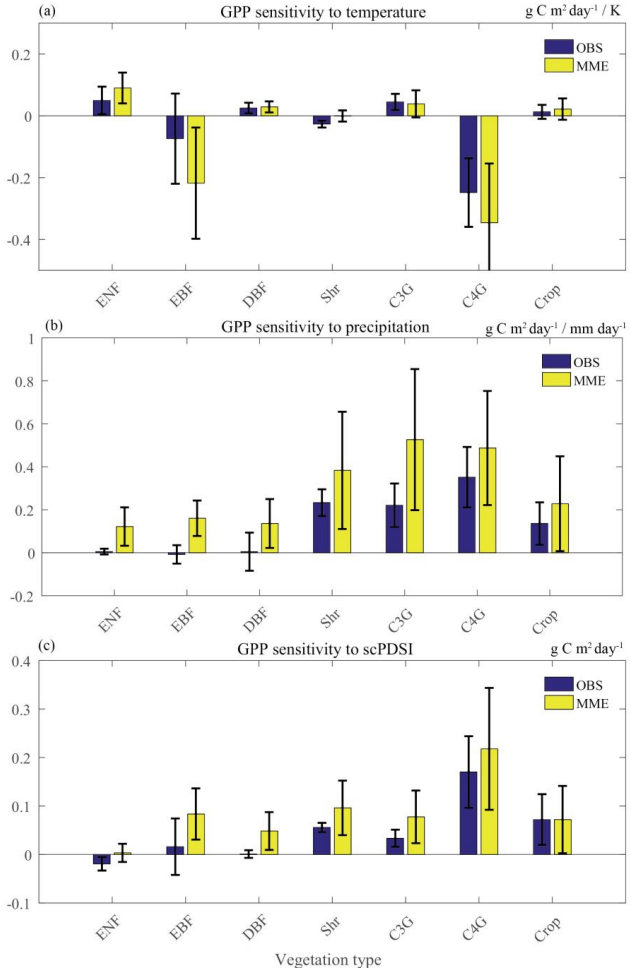

Fig. 4. Sensitivities of GPP to meteorological variables across vegetation types. The regression coefficients are calculated between GPP and (a) T2M, (b) PRE, and (c) scPDSI for both observations (blue) and model simulations (yellow). The figure presents the mean values from three observational datasets and multiple models, with errorbars indicating one standard deviation for either observations or models.

3.3 GPP responses to extreme warming and drought

We examined GPP responses to extreme high temperature and drought conditions (Fig. 5). Observations showed that extreme high temperatures moderately increased GPP in high latitudes of the NH, but weakened GPP in low latitudes, particularly in the SH (Fig. 5a). The model ensemble reproduced this spatial pattern. From a latitudinal perspective, observed and simulated GPP responses were largely consistent, with limited differences in the magnitude of fluctuations. Globally, observed GPP generally exhibited a negative response to extreme drought, a pattern that

https://doi.org/10.5194/egusphere-2025-1515
Preprint. Discussion started: 24 April 2025

was well reproduced by the MME. However, the MME tended to overestimate the magnitude of the negative response compared to observations (Fig. 5b).

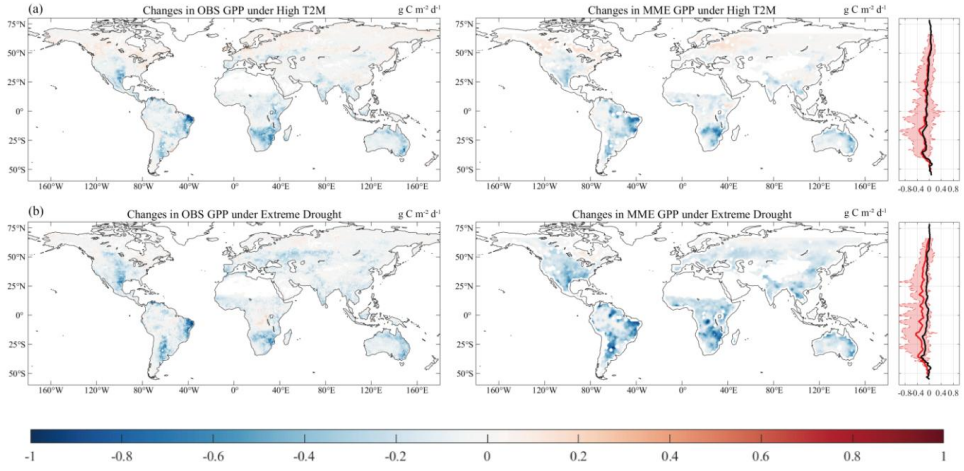

Fig. 5. Response of GPP to extreme (a) warming and (b) drought events averaged for observational datasets (GLASS, GOSIF, JUNG) and multiple model ensemble simulations. Changes in GPP are calculated as deviations during years with the (a) highest 10% of temperature or (b) lowest 10% of scPDSI at each grid point, relative to the long-term mean GPP. Latitudinal variations in GPP changes are also shown, with observational data represented in black and model simulations in red; shading indicates one standard deviation.

To better understand these responses, we analyzed GPP responses to extreme warming and drought across various datasets, models, and vegetation types (Figs S5-S6). For extreme high temperatures, GPP showed a positive response in DBF and ENF, while other vegetation types exhibited negative responses. The TRENDY models largely captured these patterns, with only 3 out of 17 models showing a negative response in DBF and all models showing a positive response in ENF (Fig. S5a). The MME also aligned reasonably well with observed averages, showing positive responses in DBF and ENF but negative responses in other vegetation types (Fig. S6a). Under extreme drought conditions, observed GPP consistently exhibited a negative response. This was well captured by the TRENDY models, though they tended to overestimate the magnitude of the responses (Fig.S5b). The MME also reproduced the observed negative responses but showed larger variability among models (Fig. S6b). It should be noted that observed GPP showed positive feedback to drought in ENF, whereas the MME showed an opposite response.

https://doi.org/10.5194/egusphere-2025-1515
Preprint. Discussion started: 24 April 2025

4 Discussion

4.1 Causes of GPP responses to meteorological factors

The response of GPP to temperature varies substantially by latitude, with a stronger positive response in high-latitude regions of the NH and an inverse relationship in low-latitude regions. This pattern is largely driven by the differing sensitivities of vegetation types to temperature changes. In high-latitude areas, which are predominantly covered by coniferous forests, low temperatures are a primary limiting factor for photosynthesis. A rise in temperature can extend the growing season, improve photosynthetic efficiency, and enhance GPP, thereby supporting the growth and carbon absorption capacity of these ecosystems (Sendall et al., 2015; Dusenge et al., 2023; Grossiord et al., 2022). In contrast, low-latitude regions are mainly comprised of EBF and grasslands. In these tropical and subtropical areas, temperatures are usually at or above the optimal thresholds for plant growth. Additional temperature increases can induce heat stress, decrease photosynthesis efficiency, and increase transpiration, leading to water deficits that further inhibit plant growth and GPP (Doughty et al., 2023; Moore et al., 2021).

Increases in precipitation and scPDSI generally indicate improved water availability, which is a fundamental constraint on plant growth, particularly in water-limited regions. The adaptability and physiological characteristics of plants to environmental conditions play a critical role in their responses. When precipitation or drought indices increase, soil moisture conditions improve, enabling plants to perform photosynthesis more effectively (Desai et al., 2022). This leads to an increase in GPP, reflecting enhanced water use efficiency and a growth advantage under adequate water conditions. However, in regions where temperature is not the primary limiting factor for plant growth, higher temperatures can exacerbate transpiration rates, resulting in water deficits (Chen et al., 2023). This dynamic explains why vegetation types that exhibit a negative correlation between GPP and temperature often show a positive correlation between GPP and precipitation or scPDSI (Fig. 2).

4.2 Performance of vegetation models

When evaluating the spatiotemporal variations of GPP, we found that models generally overestimate GPP trends compared to observations, consistent with the findings of Yang et al. (2022). During 1982-2017, the simulated GPP from the TRENDY models exhibited substantial inter-model variability (Fig. 1). Among the models, the correlation between GPP and temperature was accurately captured for most vegetation types (Fig. 3). However, models often overestimated the impact of precipitation on GPP, particularly in vegetation types such as C3G, DBF, ENF, and EBF. Moreover, GPP is typically positively correlated with the drought index, especially for non-tree species such as C3G, C4G, shrubs, and crops. The TRENDY models captured these characteristics well, but they generally overestimated the correlation between scPDSI and GPP. These overestimations are likely due to the improper parameterization of water stress and soil moisture dynamics, which leads to an exaggerated influence of water availability on GPP in the models. The MME helps to constrain inter-model variability and provides a closer estimate of the long-term GPP trend (Fig. 1). However, it still overestimates GPP sensitivities to meteorological variables, including temperature, precipitation, and drought index (Fig.4).

4.3 Uncertainties and implications

There are several uncertainties and limitations in our analyses. First, we utilized

https://doi.org/10.5194/egusphere-2025-1515
Preprint. Discussion started: 24 April 2025

observational datasets from multiple sources, including GLASS, GOSIF, and JUNG, to ensure the reliability and comprehensiveness of our results. However, these datasets inherently contain uncertainties, particularly regarding vegetation canopy structure parameters (e.g., leaf area index), which could affect the derived GPP trends and responses to meteorological variables (Prentice et al., 2024). Second, we employed multi-model simulations from TRENDY S3 run, which incorporates interannually varying meteorology and land cover. To exclude the effects of land-use change, we collected GPP data from the S2 run and re-calculated correlations/regressions with meteorological variables (Figs. S7-S8). Comparisons showed limited differences between the results from the S2 and S3 runs, supporting the robustness of our derived climatic impacts on GPP. Third, the impacts of environmental factors on GPP vary across different time scales (Zhou et al., 2023). In the short term, fluctuations in climatic factors, such as flash droughts or temperature variations, can have immediate effects on GPP. In contrast, over longer time scales, factors like vegetation adaptation, soil moisture dynamics, and long-term climate change may play more important roles. Neglecting these discrepancies in the time scales may lead to an incomplete understanding of the driving mechanisms behind GPP variations for both observations and model simulations.

Despite these limitations, this study systematically quantified the responses of GPP to different meteorological factors, and compared these responses between observational datasets and numerical models. It identified the differences in GPP responses to temperature, precipitation, and drought across various vegetation types, offering helpful insights for improving individual models. From the perspective of multi-model ensembles, the study assessed the overall performance and biases of current state-of-the-art vegetation models, as well as their ability to capture GPP responses to interannual variability and long-term climate change. These findings provide a robust foundation for understanding multi-model ensemble predictions, particularly in interpretating long-term trends and interannual fluctuations of terrestrial carbon sinks. This knowledge can support policymakers and land managers in developing scientifically informed strategies for land use and ecological conservation, ultimately promoting the resilience of ecosystem to climate change.

Data Availability Statement

The TRENDY v-11 data used for this study could be downloaded from the website (https://mdosullivan.github.io/GCB/).

Author contributions

XY conceived the project. YZ performed the data processing, conducted the analysis, and wrote the draft of the paper. XY, XL, and JZ assisted in the interpretation of the results and contributed to the discussion and improvement of the paper.

Conflict of Interest

The authors declare no conflicts of interest.

Acknowledgements

We thank all the DGVM authors in TRENDY-v11 project for providing the long-term simulation data.

https://doi.org/10.5194/egusphere-2025-1515
Preprint. Discussion started: 24 April 2025

Financial support

This research was jointly supported by the National Key Research and Development Program of China (grant no. 2023YFF0805402) and the National Natural Science Foundation of China (grant no. 42275128).

References

Beer, C., Reichstein, M., Tomelleri, E., Ciais, P., Jung, M., Carvalhais, N., Rodenbeck, C., Arain, M. A., Baldocchi, D., Bonan, G. B., Bondeau, A., Cescatti, A., Lasslop, G., Lindroth, A., Lomas, M., Luyssaert, S., Margolis, H., Oleson, K. W., Roupsard, O., Veenendaal, E., Viovy, N., Williams, C., Woodward, F. I., and Papale, D.: Terrestrial gross carbon dioxide uptake: global distribution and covariation with climate, Science, 329, 834-838, https://doi.org/10.1126/science.1184984, 2010.

Brunner, M. I. and Chartier-Rescan, C.: Drought Spatial Extent and Dependence Increase During Drought Propagation From the Atmosphere to the Hydrosphere, Geophysical Research Letters, 51, https://doi.org/10.1029/2023gl107918, 2024.

Chen, C. C. and Dominguez, F.: The Location of Large-Scale Soil Moisture Anomalies Affects Moisture Transport and Precipitation Over Southeastern South America, Geophysical Research Letters, 51, https://doi.org/10.1029/2023gl106777, 2024.

Chen, W., Wang, S., Wang, J., Xia, J., Luo, Y., Yu, G., and Niu, S.: Evidence for widespread thermal optimality of ecosystem respiration, Nat Ecol Evol, 7, 1379-1387, https://doi.org/10.1038/s41559-023-02121-w, 2023.

Clark, D. B., Mercado, L. M., Sitch, S., Jones, C. D., Gedney, N., Best, M. J., Pryor, M., Rooney, G. G., Essery, R. L. H., Blyth, E., Boucher, O., Harding, R. J., Huntingford, C., and Cox, P. M.: The Joint UK Land Environment Simulator (JULES), model description – Part 2: Carbon fluxes and vegetation dynamics, Geoscientific Model Development, 4, 701-722, https://doi.org/10.5194/gmd-4-701-2011, 2011.

Desai, A. R., Murphy, B. A., Wiesner, S., Thom, J., Butterworth, B. J., Koupaei-Abyazani, N., Muttaqin, A., Paleri, S., Talib, A., Turner, J., Mineau, J., Merrelli, A., Stoy, P., and Davis, K.: Drivers of Decadal Carbon Fluxes Across Temperate Ecosystems, J Geophys Res Biogeosci, 127, e2022JG007014, https://doi.org/10.1029/2022JG007014, 2022.

Doughty, C. E., Keany, J. M., Wiebe, B. C., Rey-Sanchez, C., Carter, K. R., Middleby, K. B., Cheesman, A. W., Goulden, M. L., da Rocha, H. R., Miller, S. D., Malhi, Y., Fauset, S., Gloor, E., Slot, M., Oliveras Menor, I., Crous, K. Y., Goldsmith, G. R., and Fisher, J. B.: Tropical forests are approaching critical temperature thresholds, Nature, 621, 105-111, https://doi.org/10.1038/s41586-023-06391-z, 2023.

Dusenge, M. E., Warren, J. M., Reich, P. B., Ward, E. J., Murphy, B. K., Stefanski, A., Bermudez, R., Cruz, M., McLennan, D. A., King, A. W., Montgomery, R. A., Hanson, P. J., and Way, D. A.: Boreal conifers maintain carbon uptake with warming despite failure to track optimal temperatures, Nat Commun, 14, 4667, https://doi.org/10.1038/s41467-023-40248-3, 2023.

Feng, X., Liu, G., Chen, J. M., Chen, M., Liu, J., Ju, W. M., Sun, R., and Zhou, W.: Net primary productivity of China's terrestrial ecosystems from a process model driven by remote sensing, J Environ Manage, 85, 563-573, https://doi.org/10.1016/j.jenvman.2006.09.021, 2007.

https://doi.org/10.5194/egusphere-2025-1515
Preprint. Discussion started: 24 April 2025

Fernandez-Martinez, M., Vicca, S., Janssens, I. A., Ciais, P., Obersteiner, M., Bartrons, M., Sardans, J., Verger, A., Canadell, J. G., Chevallier, F., Wang, X., Bernhofer, C., Curtis, P. S., Gianelle, D., Grunwald, T., Heinesch, B., Ibrom, A., Knohl, A., Laurila, T., Law, B. E., Limousin, J. M., Longdoz, B., Loustau, D., Mammarella, I., Matteucci, G., Monson, R. K., Montagnani, L., Moors, E. J., Munger, J. W., Papale, D., Piao, S. L., and Penuelas, J.: Atmospheric deposition, CO(2), and change in the land carbon sink, Sci Rep, 7, 9632, https://doi.org/10.1038/s41598-017-08755-8, 2017.

Friedl, M. A., Sulla-Menashe, D., Tan, B., Schneider, A., Ramankutty, N., Sibley, A., and Huang, X.: MODIS Collection 5 global land cover: Algorithm refinements and characterization of new datasets, Remote Sensing of Environment, 114, 168-182, https://doi.org/10.1016/j.rse.2009.08.016, 2010.

Friedlingstein, P., O'Sullivan, M., Jones, M. W., Andrew, R. M., Gregor, L., Hauck, J., Le Quéré, C., Luijkx, I. T., Olsen, A., Peters, G. P., Peters, W., Pongratz, J., Schwingshackl, C., Sitch, S., Canadell, J. G., Ciais, P., Jackson, R. B., Alin, S. R., Alkama, R., Arneth, A., Arora, V. K., Bates, N. R., Becker, M., Bellouin, N., Bittig, H. C., Bopp, L., Chevallier, F., Chini, L. P., Cronin, M., Evans, W., Falk, S., Feely, R. A., Gasser, T., Gehlen, M., Gkritzalis, T., Gloege, L., Grassi, G., Gruber, N., Gürses, Ö., Harris, I., Hefner, M., Houghton, R. A., Hurtt, G. C., Iida, Y., Ilyina, T., Jain, A. K., Jersild, A., Kadono, K., Kato, E., Kennedy, D., Klein Goldewijk, K., Knauer, J., Korsbakken, J. I., Landschützer, P., Lefèvre, N., Lindsay, K., Liu, J., Liu, Z., Marland, G., Mayot, N., McGrath, M. J., Metzl, N., Monacci, N. M., Munro, D. R., Nakaoka, S.-I., Niwa, Y., O'Brien, K., Ono, T., Palmer, P. I., Pan, N., Pierrot, D., Pocock, K., Poulter, B., Resplandy, L., Robertson, E., Rödenbeck, C., Rodriguez, C., Rosan, T. M., Schwinger, J., Séférian, R., Shutler, J. D., Skjelvan, I., Steinhoff, T., Sun, Q., Sutton, A. J., Sweeney, C., Takao, S., Tanhua, T., Tans, P. P., Tian, X., Tian, H., Tilbrook, B., Tsujino, H., Tubiello, F., van der Werf, G. R., Walker, A. P., Wanninkhof, R., Whitehead, C., Willstrand Wranne, A., Wright, R., Yuan, W., Yue, C., Yue, X., Zaehle, S., Zeng, J., and Zheng, B.: Global Carbon Budget 2022, Earth System Science Data, 14, 4811-4900, https://doi.org/10.5194/essd-14-4811-2022, 2022.

Granier, A., Reichstein, M., Bréda, N., Janssens, I. A., Falge, E., Ciais, P., Grünwald, T., Aubinet, M., Berbigier, P., Bernhofer, C., Buchmann, N., Facini, O., Grassi, G., Heinesch, B., Ilvesniemi, H., Keronen, P., Knohl, A., Köstner, B., Lagergren, F., Lindroth, A., Longdoz, B., Loustau, D., Mateus, J., Montagnani, L., Nys, C., Moors, E., Papale, D., Peiffer, M., Pilegaard, K., Pita, G., Pumpanen, J., Rambal, S., Rebmann, C., Rodrigues, A., Seufert, G., Tenhunen, J., Vesala, T., and Wang, Q.: Evidence for soil water control on carbon and water dynamics in European forests during the extremely dry year: 2003, Agricultural and Forest Meteorology, 143, 123-145, https://doi.org/10.1016/j.agrformet.2006.12.004, 2007.

Grossiord, C., Bachofen, C., Gisler, J., Mas, E., Vitasse, Y., and Didion-Gency, M.: Warming may extend tree growing seasons and compensate for reduced carbon uptake during dry periods, Journal of Ecology, 110, 1575-1589, https://doi.org/10.1111/1365-2745.13892, 2022.

Harper, A. B., Wiltshire, A. J., Cox, P. M., Friedlingstein, P., Jones, C. D., Mercado, L. M., Sitch, S., Williams, K., and Duran-Rojas, C.: Vegetation distribution and terrestrial carbon cycle in a carbon cycle configuration of JULES4.6 with new plant functional types, Geoscientific Model Development, 11, 2857-2873, https://doi.org/10.5194/gmd-11-2857-2018, 2018.

https://doi.org/10.5194/egusphere-2025-1515
Preprint. Discussion started: 24 April 2025

Haverd, V., Smith, B., Cook, G. D., Briggs, P. R., Nieradzik, L., Roxburgh, S. H., Liedloff, A., Meyer, C. P., and Canadell, J. G.: A stand-alone tree demography and landscape structure module for Earth system models, Geophysical Research Letters, 40, 5234-5239, https://doi.org/10.1002/grl.50972, 2013.

Huete, A., Didan, K., Miura, T., Rodriguez, E. P., Gao, X., and Ferreira, L. G.: Overview of the radiometric and biophysical performance of the MODIS vegetation indices, Remote Sensing of Environment, 83, 195-213, https://doi.org/10.1016/S0034-4257(02)00096-2, 2002.

Ito, A.: Changing ecophysiological processes and carbon budget in East Asian ecosystems under near-future changes in climate: implications for long-term monitoring from a process-based model, J Plant Res, 123, 577-588, https://doi.org/10.1007/s10265-009-0305-x, 2010.

Jain, A. K. and Yang, X.: Modeling the effects of two different land cover change data sets on the carbon stocks of plants and soils in concert with CO2 and climate change, Global Biogeochemical Cycles, 19, https://doi.org/10.1029/2004gb002349, 2005.

Jiao, D., Xu, N., Yang, F., and Xu, K.: Evaluation of spatial-temporal variation performance of ERA5 precipitation data in China, Sci Rep, 11, 17956, https://doi.org/10.1038/s41598-021-97432-y, 2021.

Jung, M., Reichstein, M., and Bondeau, A.: Towards global empirical upscaling of FLUXNET eddy covariance observations: validation of a model tree ensemble approach using a biosphere model, Biogeosciences, 6, 2001-2013, https://doi.org/10.5194/bg-6-2001-2009, 2009.

Jung, M., Reichstein, M., Margolis, H. A., Cescatti, A., Richardson, A. D., Arain, M. A., Arneth, A., Bernhofer, C., Bonal, D., Chen, J., Gianelle, D., Gobron, N., Kiely, G., Kutsch, W., Lasslop, G., Law, B. E., Lindroth, A., Merbold, L., Montagnani, L., Moors, E. J., Papale, D., Sottocornola, M., Vaccari, F., and Williams, C.: Global patterns of land-atmosphere fluxes of carbon dioxide, latent heat, and sensible heat derived from eddy covariance, satellite, and meteorological observations, Journal of Geophysical Research, 116, https://doi.org/10.1029/2010jg001566, 2011.

Kato, E., Kinoshita, T., Ito, A., Kawamiya, M., and Yamagata, Y.: Evaluation of spatially explicit emission scenario of land-use change and biomass burning using a process-based biogeochemical model, Journal of Land Use Science, 8, 104-122, https://doi.org/10.1080/1747423x.2011.628705, 2013.

Krinner, G., Viovy, N., de Noblet-Ducoudré, N., Ogée, J., Polcher, J., Friedlingstein, P., Ciais, P., Sitch, S., and Prentice, I. C.: A dynamic global vegetation model for studies of the coupled atmosphere-biosphere system, Global Biogeochemical Cycles, 19, https://doi.org/10.1029/2003gb002199, 2005.

Kucharik, C. J., Foley, J. A., Delire, C., Fisher, V. A., Coe, M. T., Lenters, J. D., Young-Molling, C., Ramankutty, N., Norman, J. M., and Gower, S. T.: Testing the performance of a dynamic global ecosystem model: Water balance, carbon balance, and vegetation structure, Global Biogeochemical Cycles, 14, 795-825, https://doi.org/10.1029/1999gb001138, 2000.

Lawrence, D. M., Fisher, R. A., Koven, C. D., Oleson, K. W., Swenson, S. C., Bonan, G., Collier, N., Ghimire, B., van Kampenhout, L., Kennedy, D., Kluzek, E., Lawrence, P. J., Li, F., Li, H., Lombardozzi, D., Riley, W. J., Sacks, W. J., Shi, M., Vertenstein, M., Wieder, W. R., Xu, C., Ali, A. A., Badger, A. M., Bisht, G., van den Broeke, M., Brunke, M. A., Burns, S. P., Buzan, J., Clark, M., Craig, A., Dahlin, K., Drewniak, B., Fisher, J. B., Flanner, M., Fox, A. M.,

https://doi.org/10.5194/egusphere-2025-1515
Preprint. Discussion started: 24 April 2025

Gentine, P., Hoffman, F., Keppel-Aleks, G., Knox, R., Kumar, S., Lenaerts, J., Leung, L. R., Lipscomb, W. H., Lu, Y., Pandey, A., Pelletier, J. D., Perket, J., Randerson, J. T., Ricciuto, D. M., Sanderson, B. M., Slater, A., Subin, Z. M., Tang, J., Thomas, R. Q., Val Martin, M., and Zeng, X.: The Community Land Model Version 5: Description of New Features, Benchmarking, and Impact of Forcing Uncertainty, Journal of Advances in Modeling Earth Systems, 11, 4245-4287, https://doi.org/10.1029/2018ms001583, 2019.

Le Quéré, C., Andrew, R. M., Friedlingstein, P., Sitch, S., Pongratz, J., Manning, A. C., Korsbakken, J. I., Peters, G. P., Canadell, J. G., Jackson, R. B., Boden, T. A., Tans, P. P., Andrews, O. D., Arora, V. K., Bakker, D. C. E., Barbero, L., Becker, M., Betts, R. A., Bopp, L., Chevallier, F., Chini, L. P., Ciais, P., Cosca, C. E., Cross, J., Currie, K., Gasser, T., Harris, I., Hauck, J., Haverd, V., Houghton, R. A., Hunt, C. W., Hurtt, G., Ilyina, T., Jain, A. K., Kato, E., Kautz, M., Keeling, R. F., Klein Goldewijk, K., Körtzinger, A., Landschützer, P., Lefèvre, N., Lenton, A., Lienert, S., Lima, I., Lombardozzi, D., Metzl, N., Millero, F., Monteiro, P. M. S., Munro, D. R., Nabel, J. E. M. S., Nakaoka, S.-i., Nojiri, Y., Padin, X. A., Peregon, A., Pfeil, B., Pierrot, D., Poulter, B., Rehder, G., Reimer, J., Rödenbeck, C., Schwinger, J., Séférian, R., Skjelvan, I., Stocker, B. D., Tian, H., Tilbrook, B., Tubiello, F. N., van der Laan-Luijkx, I. T., van der Werf, G. R., van Heuven, S., Viovy, N., Vuichard, N., Walker, A. P., Watson, A. J., Wiltshire, A. J., Zaehle, S., and Zhu, D.: Global Carbon Budget 2017, Earth System Science Data, 10, 405-448, https://doi.org/10.5194/essd-10-405-2018, 2018.

Leng, J., Chen, J. M., Li, W., Luo, X., Xu, M., Liu, J., Wang, R., Rogers, C., Li, B., and Yan, Y.: Global datasets of hourly carbon and water fluxes simulated using a satellite-based process model with dynamic parameterizations, Earth System Science Data, 16, 1283-1300, https://doi.org/10.5194/essd-16-1283-2024, 2024.

Li and Xiao: Mapping Photosynthesis Solely from Solar-Induced Chlorophyll Fluorescence: A Global, Fine-Resolution Dataset of Gross Primary Production Derived from OCO-2, Remote Sensing, 11, https://doi.org/10.3390/rs11212563, 2019.

Liang, C., Zhang, M., Wang, Z., Xiang, X., Gong, H., Wang, K., and Liu, H.: The strengthened impact of water availability at interannual and decadal time scales on vegetation GPP, Glob Chang Biol, 30, e17138, https://doi.org/10.1111/gcb.17138, 2024a.

Liang, S., Zhao, X., Liu, S., Yuan, W., Cheng, X., Xiao, Z., Zhang, X., Liu, Q., Cheng, J., Tang, H., Qu, Y., Bo, Y., Qu, Y., Ren, H., Yu, K., and Townshend, J.: A long-term Global LAnd Surface Satellite (GLASS) data-set for environmental studies, International Journal of Digital Earth, 6, 5-33, https://doi.org/10.1080/17538947.2013.805262, 2013.

Liang, S., He, T., Huang, J., Jia, A., Zhang, Y., Cao, Y., Chen, X., Chen, X., Cheng, J., Jiang, B., Jin, H., Li, A., Li, S., Li, X., Liu, L., Liu, X., Ma, H., Ma, Y., Song, D.-X., Sun, L., Yao, Y., Yuan, W., Zhang, G., Zhang, Y., and Song, L.: Advancements in high-resolution land surface satellite products: A comprehensive review of inversion algorithms, products and challenges, Science of Remote Sensing, 10, https://doi.org/10.1016/j.srs.2024.100152, 2024b.

Liu, Y., Zhou, Y., Ju, W., Wang, S., Wu, X., He, M., and Zhu, G.: Impacts of droughts on carbon sequestration by China's terrestrial ecosystems from 2000 to 2011, Biogeosciences, 11, 2583-2599, https://doi.org/10.5194/bg-11-2583-2014, 2014.

Ma, H. and Liang, S.: Development of the GLASS 250-m leaf area index product (version 6) from MODIS data using the bidirectional LSTM deep learning model, Remote Sensing of Environment, 273, https://doi.org/10.1016/j.rse.2022.112985, 2022.

https://doi.org/10.5194/egusphere-2025-1515
Preprint. Discussion started: 24 April 2025

Melton, J. R., Arora, V. K., Wisernig-Cojoc, E., Seiler, C., Fortier, M., Chan, E., and Teckentrup, L.: CLASSIC v1.0: the open-source community successor to the Canadian Land Surface Scheme (CLASS) and the Canadian Terrestrial Ecosystem Model (CTEM) – Part 1: Model framework and site-level performance, Geoscientific Model Development, 13, 2825-2850, https://doi.org/10.5194/gmd-13-2825-2020, 2020.

Moore, C. E., Meacham-Hensold, K., Lemonnier, P., Slattery, R. A., Benjamin, C., Bernacchi, C. J., Lawson, T., and Cavanagh, A. P.: The effect of increasing temperature on crop photosynthesis: from enzymes to ecosystems, J Exp Bot, 72, 2822-2844, https://doi.org/10.1093/jxb/erab090, 2021.

Muñoz-Sabater, J., Dutra, E., Agustí-Panareda, A., Albergel, C., Arduini, G., Balsamo, G., Boussetta, S., Choulga, M., Harrigan, S., Hersbach, H., Martens, B., Miralles, D. G., Piles, M., Rodríguez-Fernández, N. J., Zsoter, E., Buontempo, C., and Thépaut, J.-N.: ERA5-Land: a state-of-the-art global reanalysis dataset for land applications, Earth System Science Data, 13, 4349-4383, https://doi.org/10.5194/essd-13-4349-2021, 2021.

Piao, S., Sitch, S., Ciais, P., Friedlingstein, P., Peylin, P., Wang, X., Ahlström, A., Anav, A., Canadell, J. G., Cong, N., Huntingford, C., Jung, M., Levis, S., Levy, P. E., Li, J., Lin, X., Lomas, M. R., Lu, M., Luo, Y., Ma, Y., Myneni, R. B., Poulter, B., Sun, Z., Wang, T., Viovy, N., Zaehle, S., and Zeng, N.: Evaluation of terrestrial carbon cycle models for their response to climate variability and to CO2 trends, Global Change Biology, 19, 2117-2132, https://doi.org/10.1111/gcb.12187, 2013.

Pinker, R. T., Zhao, M., Wang, H., and Wood, E. F.: Impact of satellite based PAR on estimates of terrestrial net primary productivity, International Journal of Remote Sensing, 31, 5221-5237, https://doi.org/10.1080/01431161.2010.496474, 2010.

Poulter, B., Frank, D., Ciais, P., Myneni, R. B., Andela, N., Bi, J., Broquet, G., Canadell, J. G., Chevallier, F., Liu, Y. Y., Running, S. W., Sitch, S., and van der Werf, G. R.: Contribution of semi-arid ecosystems to interannual variability of the global carbon cycle, Nature, 509, 600-603, https://doi.org/10.1038/nature13376, 2014.

Prentice, I. C., Balzarolo, M., Bloomfield, K. J., Chen, J. M., Dechant, B., Ghent, D., Janssens, I. A., Luo, X., Morfopoulos, C., Ryu, Y., Vicca, S., and van Hoolst, R.: Principles for satellite monitoring of vegetation carbon uptake, Nature Reviews Earth & Environment, 5, 818-832, https://doi.org/10.1038/s43017-024-00601-6, 2024.

Reick, C. H., Gayler, V., Goll, D., Hagemann, S., Heidkamp, M., and Nabel, J. E. M. S.: JSBACH 3 - The land component of the MPI Earth System Model: documentation of version 3.2, Berichte zur Erdsystemforschung, https://doi.org/10.17617/2.3279802, 2021.

Sendall, K. M., Reich, P. B., Zhao, C., Jihua, H., Wei, X., Stefanski, A., Rice, K., Rich, R. L., and Montgomery, R. A.: Acclimation of photosynthetic temperature optima of temperate and boreal tree species in response to experimental forest warming, Global Change Biology, 21, 1342-1357, https://doi.org/10.1111/gcb.12781, 2015.

Shim, C., Hong, J., Hong, J., Kim, Y., Kang, M., Malla Thakuri, B., Kim, Y., and Chun, J.: Evaluation of MODIS GPP over a complex ecosystem in East Asia: A case study at Gwangneung flux tower in Korea, Advances in Space Research, 54, 2296-2308, https://doi.org/10.1016/j.asr.2014.08.031, 2014.

Sitch, S., Smith, B., Prentice, I. C., Arneth, A., Bondeau, A., Cramer, W., Kaplan, J. O., Levis, S., Lucht, W., Sykes, M. T., Thonicke, K., and Venevsky, S.: Evaluation of ecosystem dynamics,

https://doi.org/10.5194/egusphere-2025-1515
Preprint. Discussion started: 24 April 2025

plant geography and terrestrial carbon cycling in the LPJ dynamic global vegetation model, Global Change Biology, 9, 161-185, https://doi.org/10.1046/j.1365-2486.2003.00569.x, 2003.

Sitch, S., O'Sullivan, M., Robertson, E., Friedlingstein, P., Albergel, C., Anthoni, P., Arneth, A., Arora, V. K., Bastos, A., Bastrikov, V., Bellouin, N., Canadell, J. G., Chini, L., Ciais, P., Falk, S., Harris, I., Hurtt, G., Ito, A., Jain, A. K., Jones, M. W., Joos, F., Kato, E., Kennedy, D., Klein Goldewijk, K., Kluzek, E., Knauer, J., Lawrence, P. J., Lombardozzi, D., Melton, J. R., Nabel, J. E. M. S., Pan, N., Peylin, P., Pongratz, J., Poulter, B., Rosan, T. M., Sun, Q., Tian, H., Walker, A. P., Weber, U., Yuan, W., Yue, X., and Zaehle, S.: Trends and Drivers of Terrestrial Sources and Sinks of Carbon Dioxide: An Overview of the TRENDY Project, Global Biogeochemical Cycles, 38, https://doi.org/10.1029/2024gb008102, 2024.

Smith, B., Prentice, I. C., and Sykes, M. T.: Representation of vegetation dynamics in the modelling of terrestrial ecosystems: comparing two contrasting approaches within European climate space, Global Ecology and Biogeography, 10, https://doi.org/10.1046/j.1466-822X.2001.t01-1-00256.x, 2001.

Spahni, R., Joos, F., Stocker, B. D., Steinacher, M., and Yu, Z. C.: Transient simulations of the carbon and nitrogen dynamics in northern peatlands: from the Last Glacial Maximum to the 21st century, Climate of the Past, 9, 1287-1308, https://doi.org/10.5194/cp-9-1287-2013, 2013.

Sun, G., Hu, Z., Ma, Y., Xie, Z., Yang, S., and Wang, J.: Analysis of local land-atmosphere coupling in rainy season over a typical underlying surface in Tibetan Plateau based on field measurements and ERA5, Atmospheric Research, 243, https://doi.org/10.1016/j.atmosres.2020.105025, 2020.

Tang, R., He, B., Chen, H. W., Chen, D., Chen, Y., Fu, Y. H., Yuan, W., Li, B., Li, Z., Guo, L., Hao, X., Sun, L., Liu, H., Sun, C., and Yang, Y.: Increasing terrestrial ecosystem carbon release in response to autumn cooling and warming, Nature Climate Change, 12, 380-385, https://doi.org/10.1038/s41558-022-01304-w, 2022.

Tian, C., Yue, X., Zhou, H., Lei, Y., Ma, Y., and Cao, Y.: Projections of changes in ecosystem productivity under 1.5 °C and 2 °C global warming, Global and Planetary Change, 205, https://doi.org/10.1016/j.gloplacha.2021.103588, 2021.

Tian, H., Chen, G., Lu, C., Xu, X., Ren, W., Zhang, B., Banger, K., Tao, B., Pan, S., Liu, M., Zhang, C., Bruhwiler, L., and Wofsy, S.: Global methane and nitrous oxide emissions from terrestrial ecosystems due to multiple environmental changes, Ecosystem Health and Sustainability, 1, 1-20, https://doi.org/10.1890/ehs14-0015.1, 2015.

van der Schrier, G., Barichivich, J., Briffa, K. R., and Jones, P. D.: A scPDSI-based global data set of dry and wet spells for 1901–2009, Journal of Geophysical Research: Atmospheres, 118, 4025-4048, https://doi.org/10.1002/jgrd.50355, 2013.

Walker, A. P., Quaife, T., van Bodegom, P. M., De Kauwe, M. G., Keenan, T. F., Joiner, J., Lomas, M. R., MacBean, N., Xu, C., Yang, X., and Woodward, F. I.: The impact of alternative trait-scaling hypotheses for the maximum photosynthetic carboxylation rate (V(cmax)) on global gross primary production, New Phytol, 215, 1370-1386, https://doi.org/10.1111/nph.14623, 2017.

https://doi.org/10.5194/egusphere-2025-1515
Preprint. Discussion started: 24 April 2025

Wang, K., Sun, J., and Nie, Y.: Spring extratropical cyclones over the Mongolian region in the ERA5 reanalysis: climatology and variability, Climate Dynamics, https://doi.org/10.1007/s00382-024-07369-x, 2024.

Wang, Y.-R., Hessen, D. O., Samset, B. H., and Stordal, F.: Evaluating global and regional land warming trends in the past decades with both MODIS and ERA5-Land land surface temperature data, Remote Sensing of Environment, 280, https://doi.org/10.1016/j.rse.2022.113181, 2022.

Wei, X., He, W., Zhou, Y., Cheng, N., Xiao, J., Bi, W., Liu, Y., Sun, S., and Ju, W.: Increased Sensitivity of Global Vegetation Productivity to Drought Over the Recent Three Decades, Journal of Geophysical Research: Atmospheres, 128, https://doi.org/10.1029/2022jd037504, 2023.

Wells, N., Goddard, S., and Hayes, M. J.: A Self-Calibrating Palmer Drought Severity Index, Journal of Climate, 17, 2335-2351, https://doi.org/10.1175/1520-0442(2004)017<2335:ASPDSI>2.0.CO;2, 2004.

Wu, D., Liu, D., Wang, T., Ding, J., He, Y., Ciais, P., Zhang, G., and Piao, S.: Carbon turnover times shape topsoil carbon difference between Tibetan Plateau and Arctic tundra, Sci Bull (Beijing), 66, 1698-1704, https://doi.org/10.1016/j.scib.2021.04.019, 2021.

Wu, X., Wang, G., Yao, R., Wang, L., Yu, D., and Gui, X.: Investigating Surface Urban Heat Islands in South America Based on MODIS Data from 2003–2016, Remote Sensing, 11, https://doi.org/10.3390/rs11101212, 2019.

Xiao, J., Chevallier, F., Gomez, C., Guanter, L., Hicke, J. A., Huete, A. R., Ichii, K., Ni, W., Pang, Y., Rahman, A. F., Sun, G., Yuan, W., Zhang, L., and Zhang, X.: Remote sensing of the terrestrial carbon cycle: A review of advances over 50 years, Remote Sensing of Environment, 233, https://doi.org/10.1016/j.rse.2019.111383, 2019.

Yang, R., Wang, J., Zeng, N., Sitch, S., Tang, W., McGrath, M. J., Cai, Q., Liu, D., Lombardozzi, D., Tian, H., Jain, A. K., and Han, P.: Divergent historical GPP trends among state-of-the-art multi-model simulations and satellite-based products, Earth System Dynamics, 13, 833-849, https://doi.org/10.5194/esd-13-833-2022, 2022.

Yue, X. and Unger, N.: The Yale Interactive terrestrial Biosphere model version 1.0: description, evaluation and implementation into NASA GISS ModelE2, Geoscientific Model Development, 8, 2399-2417, https://doi.org/10.5194/gmd-8-2399-2015, 2015.

Yue, X., Zhou, H., Tian, C., Ma, Y., Hu, Y., Gong, C., Zheng, H., and Liao, H.: Development and evaluation of the interactive Model for Air Pollution and Land Ecosystems (iMAPLE) version 1.0, Geoscientific Model Development, 17, 4621-4642, https://doi.org/10.5194/gmd-17-4621-2024, 2024.

Zaehle, S. and Friend, A. D.: Carbon and nitrogen cycle dynamics in the O-CN land surface model: 1. Model description, site-scale evaluation, and sensitivity to parameter estimates, Global Biogeochemical Cycles, 24, https://doi.org/10.1029/2009gb003521, 2010.

Zeng, X., Hu, Z., Chen, A., Yuan, W., Hou, G., Han, D., Liang, M., Di, K., Cao, R., and Luo, D.: The global decline in the sensitivity of vegetation productivity to precipitation from 2001 to 2018, Glob Chang Biol, 28, 6823-6833, https://doi.org/10.1111/gcb.16403, 2022.

Zhang, J., Zhou, X., Yang, S., and Ao, Y.: Spatiotemporal Variations in Evapotranspiration and Their Driving Factors in Southwest China between 2003 and 2020, Remote Sensing, 15, https://doi.org/10.3390/rs15184418, 2023.

https://doi.org/10.5194/egusphere-2025-1515
Preprint. Discussion started: 24 April 2025

747 Zhang, X., Wang, Y. P., Peng, S., Rayner, P. J., Ciais, P., Silver, J. D., Piao, S., Zhu, Z., Lu, X., and
748 Zheng, X.: Dominant regions and drivers of the variability of the global land carbon sink
749 across timescales, Glob Chang Biol, 24, 3954-3968, https://doi.org/10.1111/gcb.14275, 2018.
750 Zhang, Y., Piao, S., Sun, Y., Rogers, B. M., Li, X., Lian, X., Liu, Z., Chen, A., and Peñuelas, J.:
751 Future reversal of warming-enhanced vegetation productivity in the Northern Hemisphere,
752 Nature Climate Change, 12, 581-586, https://doi.org/10.1038/s41558-022-01374-w, 2022.
753 Zhou, H., Yue, X., Wang, B., Tian, C., Lu, X., Zhu, J., and Cao, Y.: Distinguishing the main
754 climatic drivers to the variability of gross primary productivity at global FLUXNET sites,
755 Environmental Research Letters, 18, https://doi.org/10.1088/1748-9326/ad059c, 2023.
756 Zhou, S., Zhang, Y., Caylor, K. K., Luo, Y., Xiao, X., Ciais, P., Huang, Y., and Wang, G.:
757 Explaining inter-annual variability of gross primary productivity from plant phenology and
758 physiology, Agricultural and Forest Meteorology, 226-227, 246-256,
759 https://doi.org/10.1016/j.agrformet.2016.06.010, 2016.
760 Zscheischler, J., Mahecha, M. D., von Buttlar, J., Harmeling, S., Jung, M., Rammig, A.,
761 Randerson, J. T., Schölkopf, B., Seneviratne, S. I., Tomelleri, E., Zaehle, S., and Reichstein,
762 M.: A few extreme events dominate global interannual variability in gross primary production,
763 Environmental Research Letters, 9, https://doi.org/10.1088/1748-9326/9/3/035001, 2014.
764